Int. J.Nano Dimens. 5(4): 341-349, Autumn 2014
ISSN: 2008-8868

Contents list available at **IJND**

International Journal of Nano Dimension

Journal homepage: *www.IJND.ir*

Ex-situ studies on calcinations of structural, optical and morphological properties of post-growth nanoparticles CeO_2 by HRTEM and SAED

B. Sathyaseelan[1]
S. Sambasivam[2]
T. Alagesan[3]
K. Sivakumar[4,*]

[1]*Department of Physics, University college of Engineering Arni (A constituent college of Anna University Chennai) Arni 632 317, Tamilnadu, India.*
[2]*Department of Physics, Pukyong National University, Busan-608 737, South Korea.*
[3]*Department of Physics, Presidency College, Chennai 600 005, Tamil Nadu, India.*
[4]*Department of Physics, Anna University, Chennai-600025, Tamilnadu, India.*

Received 14 March 2013
Accepted 27 August 2013

* Corresponding author:
K.Sivakumar
Department of Physics, Anna University, Chennai-600025,Tamilnadu, India.
Tel +91 4422208700
Fax +91 4422208700
Email ksivakumar@annauniv.edu

ABSTRACT

Nanocrystalline particles of Cerium Oxide (CeO_2) have been prepared by the chemical precipitation method using Cerium nitrate and Urea with a molar ratio of 1:2. The results revealed that the formation of CeO_2 fine particles is influenced by molar ratio of metal nitrates to fuel. Well faceted CeO_2 nanoparticles, were synthesized by thermal-assisted dissociation method at reflux temperature in a short period of time. A possible mechanism for synthesis of such highly pure and stable nanoparticles is tentatively proposed by thermogravimetry-differential thermal analysis (TG –DTA) study. The powders were investigated by X-ray diffraction (XRD), Transmission electron microscopy (TEM), selected area electron diffraction (SAED), high resolution transmission electron microscopy (HRTEM). In addition, uniform particles, size distribution and purity of samples are highly dependent on the applied chemical precipitation method. Raman spectroscopy and Electron Diffraction Analysis confirmed the fluorite structure of bulk CeO_2.

Keywords: *Cerium Oxide; Chemical synthesis; Characterization methods; Raman spectroscopy; Transmission electron microscopy (TEM); Optical properties.*

INTRODUCTION

Synthesis and characterization of oxide-based nanoscale materials are topics of current research mainly due to their potential applications in nanoscale devices [1]. Cerium oxide (CeO_2) nanoparticles have attracted considerable attention due to their technological applications in electrolytes for solid oxide fuel cells [2-3], catalysts [4], abrasives [5-6], gas sensors [7], ultraviolet absorbents for sunscreens [8], solar cells [9] and absorbents for H_2S removal [10]. And its properties are strongly dependent on the size and size distribution of ceria nanoparticles [11]. By decreasing the grain size from macroscopic scale to nanoscale, one can expect enhanced catalytic activity, sinterability, and other properties of the material.

Generally, the performance of nanoparticles is strongly influenced by the powder characteristics like crystallite size, surface area, and the extent of agglomeration.

Several techniques have been reported for the preparation of nano-sized CeO_2 particles, like co-precipitation [12], solvothermal synthesis [13], hydrothermal technique [14-15], sonochemical [16] and combustion based synthesis [17]. The most promising alternative is the soft-chemistry route, which provides good control from the molecular precursor to the final product, apart from offering high purity and homogeneity [18-20]. Among the above methods, the precipitation method has advantages in the preparation of chemically homogeneous powders with controlled morphologies. This method is also simple and cost-effective. However, high-temperature heat treatment is needed to prepare well-crystallized powders from the precipitates, and it results in the growth of nanosized particles. Here, we report the synthesis of nanocrystalline CeO_2 by the chemical precipitation method and its structural and optical characterization.

EXPERIMENTAL

Pure CeO_2 nanoparticles were prepared by a chemical precipitation method using cerium nitrate and urea as the sources of 1:2 ratios respectively. The salts were added in de-ionized water and mixed homogeneously and refluxed for 48 hour under air atmosphere. The precipitates were washed several times with de-ionized water to remove the water-soluble impurities and free reactants and dried at 110 ◦C for 10 h. The dried product was ground using a pestle and mortar, the portions of it were at temperatures in the range of 500–1000 ºC for an hour to obtain CeO_2. The resultant powders were characterized to determine the particle size, structure and morphology. The structure of the as-prepared and CeO_2 powder samples was characterized using Powder X-ray diffraction (XRD) patterns were obtained on a Rich Siefert, Model 3000 powder diffractometer operating at 40 kV and 25 mA using CuKα1 (λ = 1.54 Å) radiation. Data were collected from 10° to 70° with a sampling interval of 0.01° per step and a counting rate of 1 s per step. The lattice parameters of the samples were calculated by the help of XRD peak fit (using XRDA software) and the average crystallite size were calculated using Scherer's formula. The TG-DTA runs were performed with a Netzsch STA 409C instrument at a heating rate of 20 °C min^{-1} from the room temperature to 800 °C, using Al_2O_3 as a reference. Band gap energies of the samples were calculated using UV–visible spectrophotometer (Lambda 20, Perkin Elmer). The size and morphology of nanocrystallites were observed through transmission electron microscopy (TEM, JEOL JEM-1200EX). Crystal lattice fringes were observed by high-resolution transmission microscope (HRTEM, JEOL 3010) with an accelerating voltage of 200 kV. The morphological features of the samples were observed by scanning electron microscope (SEM; Hitachi S-3000N). The Raman spectrum was measured with SPEX-1403 laser Raman spectrometer at room temperature. An Ar-ion laser with a wavelength of 514.5 nm in a backscattering configuration was used as an exiting source. Specific surface area, pore volume, and pore size distributions of the samples at 800 and 1000ºC were determined by N_2-adsorption and desorption isotherms. Brunauer, Emmet, and Teller (BET) model and Barret, Joyner and Hallenda (BJH) desorption method were used to obtain specific areas and porosity distribution, respectively.

RESULTS AND DISCUSSION

The XRD patterns of the as prepared and calcined CeO_2 samples are shown in Figure 1. The as prepared sample shows no XRD peaks, indicating its amorphous nature, whereas all the calcined samples exhibit XRD peaks that correspond to the (111), (200), (220), (311), and (222) planes of a cubic fluorite structure of CeO_2 as identified using the standard data JCPDS 34-0394. It is clearly seen that the reflection peaks become sharper and narrower with increasing calcination temperature, indicating that the crystal size increases and the crystallinity of CeO_2 become better-defined during the calcination process. The average crystallite sizes D of the CeO_2 samples were calculated from X-ray line broadening of the reflections of (111) using Scherrer's equation [21]

(i.e., $D = 0.9\lambda/\beta Cos\theta$

where λ is the wavelength of the X-ray radiation, K is a constant taken as 0.9, θ is the diffraction angle, and β is the full width at half-maximum (fwhm)), respectively. Figure 2 the values of lattice parameter a calculated from the XRD spectra were 5.439(3) Å, 5.443(2) Å and 5.445(3) Å for the CeO_2 samples calcined at 500, 800, and 1000 °C, respectively. The particle sizes and lattice parameters are also summarized in and Table 1. Our results are in agreement with those of Leoni et al., [22] who reported that the lattice parameter of nanocrystalline CeO2 powders changes as a function of calcination temperature. However, their sample has the lattice parameter higher than that of the standard powder (JCPDS 34-0394), and the difference tends to decrease with increasing particle size. For nanocrystalline powders, the lattice parameter has been found to vary with the particle size, and this behaviour has been explained in terms of grain surface relaxation. [22] Nanocrystalline particles or grains are supposed to possess a core-shell structure where the structure of the core is very close to that of bulk nanocrystalline cerium oxide and the surface tends to relax. The lattice parameter, therefore, increases locally at the surface. In addition, it was found that the grain surface relaxation contributes to the line broadening, thus tending to reduce the measured value of dislocation density. [23] The difference in relation between the lattice parameter and particle size observed in our CeO_2 samples and that of nanocrystalline CeO_2 powders reported by Leoni et al.[22] is possibly due to the difference in the particle surface relaxation. When the nanoparticles grow larger in the higher calcination temperature, their lattice parameter approaches that of the bulk value.

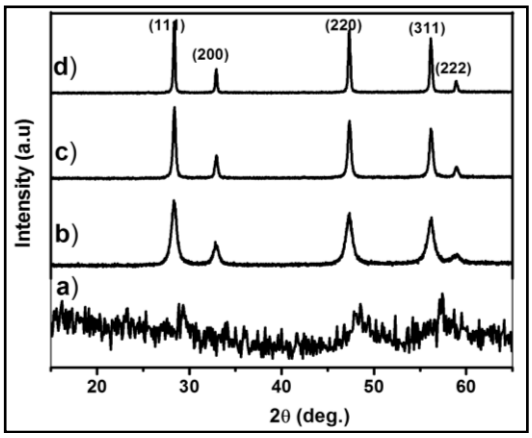

Fig. 1. Powder XRD patterns of (a) as-prepared sample and those after calcined at different temperatures, (b) 500, (c) 800 (d) 1000^{0}C for 1 h in air.

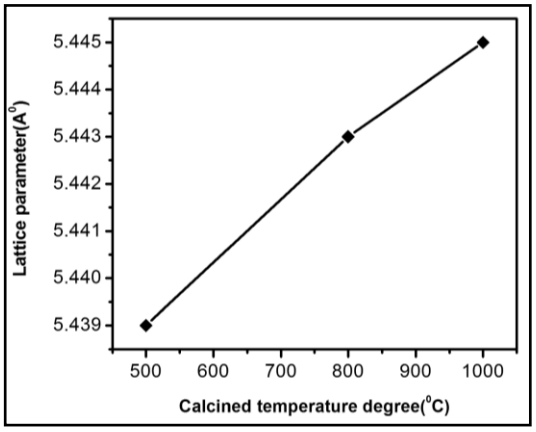

Fig. 2. Lattice parameter a measurement of various CeO_2 at different temperatures.

Table 1. Particle Sizes from XRD Line Broadening, Raman Line Broadening, and TEM, Cubic Lattice Parameter a Calculated from XRD Patterns, and Band Gap Eg Derived from UV-Vis Spectra of theCeO_2 Samples Calcined in Air at 500, 800, and 1000 °C for 2 h

Nanocrystalline CeO_2	particle size (nm)			Cubic lattice parameter a (nm)	band gap Eg (eV)
	from XRD line broadening	from Raman line broadening	from TEM		
calcined at 500 °C	15	14.5	-	5.439(3)	3.59
calcined at 800 °C	23	20.5	20-25	5.443(2)	3.55
calcined at 1000 °C	34	48.5	30-35	5.445(3)	3.51

The formation of a cubic structure in the calcined CeO_2 samples was further supported by Raman spectra. Figure 3 shows typical Raman spectra of CeO_2. The Raman active modes for the CeO_2 samples calcined at 500, 800, and 1000 ° C are 465.5, 463.8, and 462.1 cm^{-1}, respectively. These Raman active modes are attributed to a symmetrical stretching mode of the Ce-8O vibrational unit and therefore they are very sensitive to any disorder in the oxygen sublattice resulting from thermal, doping, or grain size. [24, 25]. The effect of the microstructure of CeO_2 on the shape of the Raman spectra was observed by the broadening of the line and by increasing its asymmetry, which are attributed to the reduction of the phonon lifetime in the nanocrystalline regime [24,26-28]. The Raman line broadening of CeO_2 can be described by the dependence of the half-width, Γ, on the inverse of grain size, dg, which follows a linear behaviour [24,25,28].

$$\Gamma\ (cm\text{-}1) = 10 + 124.7/dg$$

Using the above relation, we found the crystal size of the CeO_2 samples to be 14.5, 20.5 and 48.7 nm for the CeO_2 samples calcined at 500, 800, and 1000 ° C, respectively. These data are in good agreement with results obtained from X-ray line broadening, for which the calculated particle size from the Raman spectra gives a result. (See Table 1).

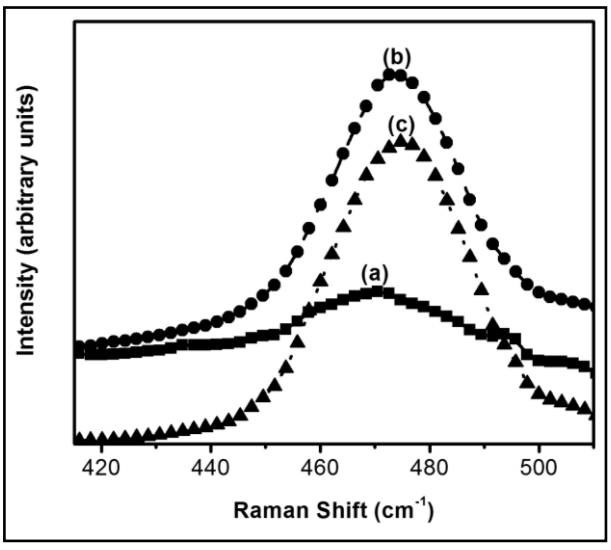

Figure 3. Raman spectra of calcined at different temperatures, (a) 500, (b) 800 (c) 1000^0C for 1 h in air.

The TGA/DTA curve of CeO_2 powders prepared by chemical precipitation method is shown in Figure 4. The process of decomposition involves three stages. In the first step, i.e. from the ambient to 210˚C, decomposition and evaporation of the absorbed water occurs, with a weight loss of 8.96%. After the adsorbed water removal from the as prepared sample, decomposition of Ce $(OH)_4$ will take place to give $CeO_2 + 2H_2O$. XRD may show small peaks of only CeO_2 as crystalline phase since amorphous Ce $(OH)_4$ will not show in XRD. The weight loss in region 210-400°C is for decomposition of Ce $(OH)_4$ with a weight loss of 9.16%. The final step from 400 to 575˚C shows decomposition of organic derivatives and the formation of CeO_2 with a weight loss of 1.36% [29]. The net weight loss of the compound was found to be 19.48%. The DTA results of the as-prepared sample show the exothermic curves to be associated with the corresponding weight loss in TG curves. The above observations are for decomposition of salts i.e., urea or Ce $(NO_3)_3.6H_2O$. When the chemical precipitation techniques are employed, it is not expected that urea or cerium nitrate will remain in the precipitate. The soluble salts will be removed while the precipitate is washed.

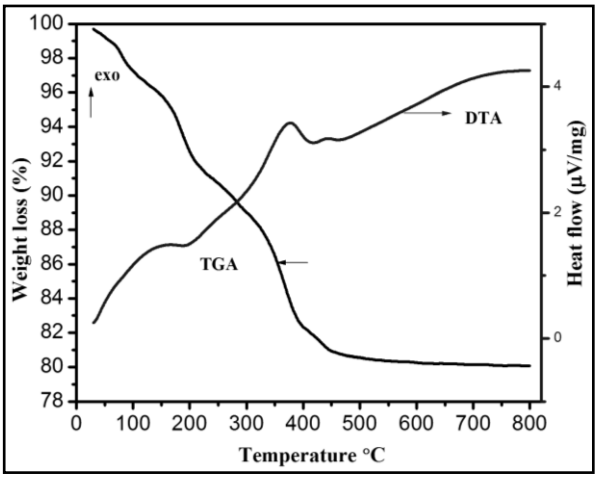

Fig. 4.TG/DTA curves of as prepared CeO_2 sample.

To reveal the correlation between the band gap energies and the grain size and morphology of the sample, the UV-Vis absorption spectra of CeO_2 nanoparticles were recorded. The optical absorption coefficient R was calculated

according to the following equation: R= (2.303 x 10^3Aρ)/lc, where A is the absorbance of the sample, ρ is the real density of CeO_2 (7.28 g cm-3), l is the path length of the quartz cell (1 cm), and c is the concentration of the ceria suspensions. [29.] The UV-Vis absorption spectra of the cerium dioxide structures were measured in ethanol suspensions (Figure 5). Both of them exhibit strong absorption bands at ca. 336 to 353 nm in the UV range, which originate from the charge-transfer between the O2p and Ce4f states in O^{2-} and Ce^{4+} [30,31]. This spectral profile indicates the charge-transfer transition of Ce^{4+} overlaps with the 4f1 f 5d1 transition of Ce^{3+}. No absorption was detected above 500 nm in wavelength. A clear blue-shifting of the absorption threshold edge can be observed for the CeO_2 nanospheres and microrods, contrasting with the bulk powder. The plots of $(RhV)^2$ vs photon energy of CeO_2 like particles are shown in Figure 6. For direct transitions, the absorption coefficient near the absorption edge can be expressed in the following equation: [32] where Ed is the band gap energy for direct transitions and hV is the photon energy. From the intersection of the extrapolated linear portion, the Ed values of the CeO_2 nanospheres, microrods, spindle-like particles, and bulk samples can be determined as 3.46, 3.62, and 3.36 eV, respectively. Compared to the no oriented polycrystalline CeO_2 (Ed) 3.19 eV determined by UV-vis spectroscopy), [33] CeO_2 nanospheres, microrods, and spindle-like structures showed an increase in Ed by a value exceeding 0.27, 0.43, and 0.17 eV, respectively. The blue-shifting phenomenon in the UV absorption spectra of CeO2 nanocrystals has attracted the interest of many researchers in recent years [34-37]. Generally, the absorption of ceria in the UV region originates from the charge-transfer transition between the O 2p and Ce 4f states in O^{2-} and Ce^{4+}. This absorption is much stronger than the 4f1-5d1 transition from the Ce^{3+} species in the mixed valence ceria system [31,36,38]. It was theoretically deduced that the value of blue-shifting resulting from the reduction of particle size is inverse proportional to the square of the size due to quantum confinement effect. Tsunekawa et al. stated that the blue shifts could also be explained by changes in the electronic band structure [37].

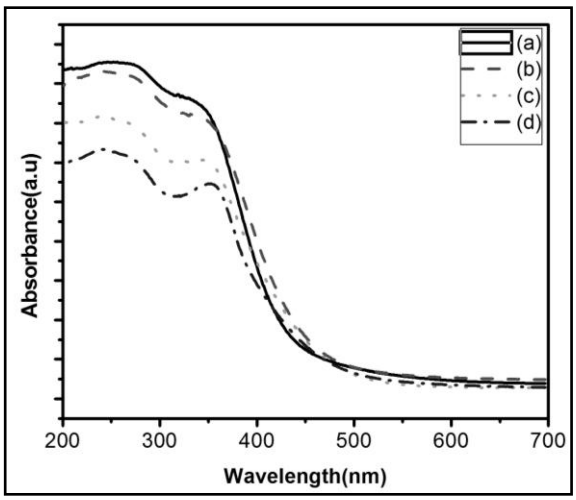

Fig. 5. Optical absorption spectra of: (a) as-prepared sample and those after calcined at different temperatures, (b) 500, (c) 800 (d) 1000^{0}C for 1 h in air.

The TEM images of the CeO_2 at temperature of 800 and 1000ºC are shown in Figure 6a and 6b. TEM images show that the particles to be aggregates with polyhedron shape and average value of around a 23 (for 800ºC) and 33 nm (for 1000ºC), which is consistent with the results observed from XRD studies. The yield of the prepared CeO_2 estimated by TEM observations is about 99.9 % relative to the samples on copper grids, and much less contents of the obtained product are nanoparticles. Thus, the high yield efficiency of this approach for the synthesis of CeO_2 can be concluded, with an ultrahigh crystallinity, outstanding morphology and an excellent yield. From the rings of selected area electron diffraction (SAED) (Figure 6c and 6d) patterns, (111), (200), (220), (311), (511) and (440) planes belonging to fluorite cubic CeO_2 is clearly visible. At the same time, the SAED patterns of the samples were consistent with the ultra-high crystallinity, and the diffraction spot could be indexed as the cubic phase. This result was in good agreement with the result of XRD. Their microstructures (i.e., uniform particles, size distribution, purity, crystallinity degree and so on) are characterized at atomic scale, especially by HRTEM, to achieve nanoparticles with controlled microstructural characteristics. Moreover, the particle size increases with temperature, indicating that the growth rate of particles is predominant over the nucleation rate [39, 40]. The fringes appearing in the micrographs allow for the identification of

the crystallographic spacing of the CeO_2 nanocrystallites that are identified in the micrographs. The fringes most frequently observed correspond respectively to the (111) crystallographic planes of CeO_2 phases. Only the fringes assigned to CeO_2 phases were observed, confirming our previous statement about a well-dispersed copper species on the support, which was revealed by Raman analysis and XRD data [41]. In further investigation, the CeO_2 nanostructures were analyzed by HRTEM in detail, and all nanoparticles showed uniform lattice fringes, meaning that no amorphous product was formed. Figure 6e and 6f is the HRTEM image of CeO_2 nanostructure, which clearly indicates that the CeO_2 is structurally uniform crystalline with ultra-high crystallinity. The interplanar spacing values are calculated from Bragg's diffraction equation using the diffraction ring diameter and the camera length of the transmission electron microscope. The calculated results indicate the fringes spacing about 0.31, 0.27, and 0.19 nm which match well with the (111), (200), and (220) planes, respectively, of the fluorite cubic CeO_2 structure that can be observed.

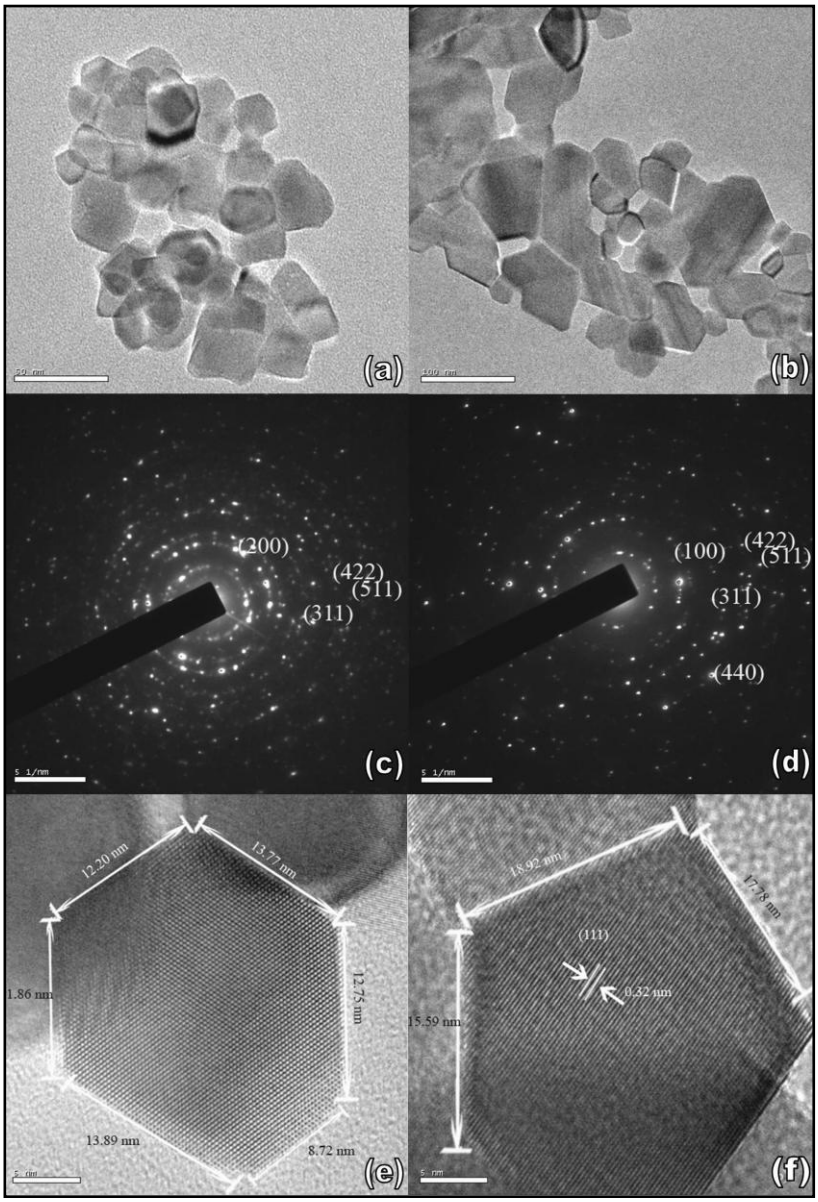

Figure 6. TEM, Electron Diffraction pattern and HRTEM micrographs of nanocrystalline CeO_2 powders in air for 1 h at [(a), (c) and (e)] 800, and [(b), (d), and (f)] 1000°C.

CONCLUSIONS

Nanocrystalline CeO_2 has been synthesized by chemical precipitation method. The X-ray diffraction (XRD) patterns, Raman spectra, and electron diffraction studies suggest the formation of CeO_2 cubic fluorite structure in all of the CeO_2 samples calcined at 500, 800, and 1000° C. All samples have networked nanocrystalline CeO_2 particles whose sizes increase with increasing calcination temperature. All samples show a strong absorption below 400 nm (3.10 eV) with a well-defined absorbance peak at around 336 to 353 nm. The estimated direct band gaps are 3.59, 3.55, and 3.51 eV for the CeO_2 samples calcined at 500, 800, and 1000 ° C, respectively. We believe that the current simple, cost-effective, and environmentally friendly synthesis method using water-soluble can be extended to prepare nanoparticles of other interesting materials.

REFERENCES

[1] Yin Y., Alivisatos A. P., (2005), Colloidal nanocrystal synthesis and the organic-inorganic interface. *Nature* 437: 664-670.

[2] Murray E. P., Tsai T., Barnett S. A., (1999). A direct-methane fuel cell with a ceria-based anode. *Nature* 400:649–651.

[3] Steele B. C. H., (2000), Materials for IT-SOFC stacks 35 years R&D: For IT-SOFC operation at 500 °C Solid State Ionics. 129: 95–110.

[4] Fu Q., Saltsburg H., .Flytzani-Stephanopoulos M., (2003), Active non metallic Au and Pt species on ceria-based water-gas shift catalyst. *Science* 301: 935–938.

[5] Lu Z. Y., Lee S. H., Gorantla V. R. K., Babu S. V., Matijevic E., (2003), Effects of mixed abrasives in chemical mechanical polishing of oxide films. *J. Mater. Res*. 18: 2323–2330.

[6] Shchukin D. G., Caruso R. A., (2004), Template Synthesis and Photocatalytic Properties of Metal Oxide Spheres Formed by Nanoparticle Infiltration. *Chem. Mater*. 16: 2287–2292.

[7] Garzon F. H., Mukundan R., Brosha E. L., (2000), Solid-state mixed potential gas sensors: Theory, experiments and challenges Solid State Ionics. 136: 633–638.

[8] Imanaka N., Masui T., Hirai H., Adachi G., (2003), Amorphous Cerium-Titanium Solid Solution Phosphate as a Novel Family of Band Gap Tunable Sunscreen Materials. *Chem. Mater*. 15: 2289–2291.

[9] Lira-Cantu M., Krebs F. C., (2006), Hybrid solar cells based on MEH-PPV and thin film semiconductor oxides TiO_2, Nb_2O_5, ZnO, CeO_2 and CeO_2-TiO_2: Performance improvement during long-time irradiation, Solar Energy Mater. *Solar Cells* 90: 2076–2086.

[10] Flytzani-Stephanopoulos M., Sakbodin M., Wang Z., (2006), Regenerative Adsorption and removal of H_2S from hot fuel gas streams by Rare earth oxides. *Science* 312: 1508–1510.

[11] Spanier J., E.Robinson R. D., Zheng F., Han S. W., Herman I. P., (2001), Size-dependent properties of CeO_2-y nanoparticles studied by Raman scattering. *Phys. ReV. B.* 64: 245407-24508.

[12] Kirk T. J., Winnick J., (1993), A Hydrogen Sulfide Solid-Oxide Fuel Cell Using Ceria Based Electrolytes. *J. Electrochem. Soc.* 140: 3494-3496.

[13] Liwu Q., Jun Z., Weimin Du., Xuefeng Q., (2009), Solvothermal synthesis, electrochemical and photocatalytic properties of monodispersed CeO_2 nanocubes Materials Chemistry and Physics. 115: 835–840.

[14] Xu J., Li G., Li L., (2008), CeO_2 nanocrystals: Seed-mediated synthesis and size control. *Mater. Res. Bull*. 43: 990-995.

[15] Kaneko K., Inoke K., Freitag B., Hungria A. B., Midgley P. A., Hansen T. W., Zhang J., Ohara S., Adschiri T., (2007), Structural and Morphological Characterization of Cerium Oxide Nanocrystals Prepared by Hydrothermal Synthesis. *Nano Lett*. 7421-425.

[16] Yin L., Wang Y., Pang G., Koltypin Y., Gedanken A., (2002), Sonochemical Synthesis of Cerium Oxide Nanoparticles—Effect of Additives and Quantum Size Effect. *J. Colloid Interf. Sci*. 246: 78-84.

[17] Bera P., Gayen A.,Hegde M. S., Lalla N. P., Spadaro L., Frusteri F., Arena F., (2003), Promoting effect of CeO_2 in combustion synthesized Pt/CeO_2 catalyst for CO oxidation. *J. Phys. Chem. B*. 107: 6122–6130.

[18] Segal D., (1997), Chemical synthesis of ceramic materials, *J. Mater. Chem*. 7: 1297–1305.

[19] Schwartz R. W., Schneller T., Waser R., Chimie C. R., (2004), Chemical solution deposition of electronic oxide films. 7: 433–461.

[20] Cushing B. L., Kolesnichenko V. L., O'Connor C. J., (2004), Recent advances in the liquid-phase syntheses of inorganic nanoparticles. *Chem. Rev*. 1043: 893–946.

[21] Cullity B. D., Stock S. R., (2001), Elements of X-ray Diffraction, 3rd ed.; Prentice Hall: Upper Saddle River, NJ.

[22] Leoni M., Maggio R. D., Polizzi S., Scardi P., (2004), X-ray diffraction methodology for the microstructural analysis of nanocrystalline powders: Application to cerium oxide. *J. Am. Ceram. Soc*. 87: 1133-1140.

[23] Scardi P., (1999), A New Whole Powder Pattern Approach. In X-ray Powder Diffraction Analysis of Real Structure of Materials, International Union of Crystallography Series; Bunge, H.-J., Fiala, J, Snyder, R. L., Eds.; Oxford University Press: Oxford, U.K., p- 570.

[24] Kosacki I., Suzuki T., Anderson H. U., Colomban P., (2002), Raman scattering and lattice defects in nanocrystalline CeO_2 thin films. *Solid State Ionics*, 149: 99-105.

[25] Kosacki I, Petrovsky V, Anderson H. U, Colomban P., (2002), Raman spectroscopy of nanocrystalline ceria and Zirconia thin films. *J. Am. Ceram. Soc*. 85: 2646–2650.

[26] Barker A. S., Sievers A., (1975), Optical studies of the vibrational properties of disordered solids. *J. ReV. Mod. Phys*. 47: S1-S179.

[27] Parayanthal P., Pollak F. H., (1984), Raman scattering in alloy semiconductors: "spatial correlation" model. *Phys. ReV. Lett*., 52: 1822-1828.

[28] Weber W. H.; Hass K. C., McBride, H., (1993), Raman study of CeO_2: Second-order scattering, lattice dynamics, and particle-size effects. *J. R. Phys. ReV. B*. 48: 178-185.

[29] Zhang Y. W., Si R., Liao C. S., Yan C. H., Xiao C. X., Kou Y., (2003), Facile Alcohol thermal Synthesis, Size-dependent Ultraviolet Absorption and Enhanced CO Conversion Activity of Ceria Nanocrystals. *J. Phys. Chem. B*. 107: 10159-10167.

[30] Tsunekawa S., Fukuda T., (1999), Blue shift in ultraviolet absorption spectra of monodisperse CeO_{2-x} nanoparticles. *J. Appl. Phys.* 87: 1318-1321.

[31] Tsunekawa S., Sahara R., Kawazoe Y., Kasuya A., (2000), Origin of the Blue Shift in Ultraviolet Absorption Spectra of Nanocrystalline CeO_2-x Particles. *Mater. Trans. JIM*. 41: 104-1107

[32] Van Leeuwen R. A., Huang C. J., Kammler D. R., Switzer J. A., (1995), Optical and Electronic Transport Properties of Electrodeposited Thallium(III) Oxide Films. *J. Phys. Chem. B*. 99: 5247-5251.

[33] Orel Z. C., Orel B., (1994), Optical Properties of Pure CeO_2 and Mixed CeO_2/SnO_2 Thin Film Coatings Phys. *Status Solid. B.* 186: K33-K36.

[34] Inoue M., Kimura M., Inui T., (1999), Transparent colloidal solution of 2 nm ceria particles. *Chem. Commun*. 11: 957-958.

[35] Yin L. X., Wang Y. Q., Pang G. S., Koltypin Y., Gedanken A., (2002), Sonochemical Synthesis of Cerium Oxide Nanoparticles—Effect of Additives and Quantum Size Effect. *J. Colloid Interface Sci.* 246: 78-84.

[36] Murata T., Sato M., Yoshida H., Morinaga K., (2005), Compositional dependence of ultraviolet fluorescence intensity of Ce3+ in silicate, borate, and phosphate glasses. *J. Non-Cryst. Solids*. 351: 312-316 ,

[37] Tsunekawa S., Wang J. T., Kawazoe Y., Kasuya A., (2003), Blue shifts in the ultraviolet absorption spectra of cerium oxide nanocrystallites. *J. Appl. Phys*. 94: 3654-3656.

[38] Tsunekawa S., Fukuda T., (1999), Blue shift in ultraviolet absorption spectra of monodisperse CeO_{2-x} nanoparticles. *J. Appl. Phys*. 87: 1318-1321. ,

[39] Wu N. C., Shi E. W., Zheng Y. Q., Li W. J., (2002), Effect of Medium on Hydrothermal Synthesis of Nanocrystalline Cerium(IV) Oxide Powders. *J. Am. Ceram. Soc*. 85: 2462-2468.

[40] Lu J., Fang Z. Z., (2006), Synthesis and Characterization of Nanoscaled Cerium (IV) Oxide via a Solid-State Mechanochemical Method. *J. Am. Ceram*. Soc. 89: 842-847.

[41] Francisco M. S. P., Nascente P. A. P., Mastelaro V. R., Florentino A. O. J., (2001), *Vac. Sci. Technol.* A 19AIP ID# 042104JVA.

Cite this article as: B. Sathyaseelan *et al.*: Ex-situ studies on calcinations of structural, optical and morphological properties of post-growth nanoparticles CeO_2 by HRTEM and SAED.
Int. J.Nano Dimens. 5(4): 341-349, Autumn 2014